APPLICATION OF MATHEMATICAL HEAT FLOW AND STRESS MODELS OF STEEL INGOT CASTING TO INVESTIGATE PANEL CRACK FORMATION

B. G. Thomas
Department of Mechanical and Industrial Engineering
University of Illinois at Urbana-Champaign
Urbana, IL 61801

I. V. Samarasekera and J. K. Brimacombe
The Center for Metallurgical Process Engineering
The University of British Columbia
Vancouver, Canada

Abstract

Mathematical models have been developed for the processing of static-cast steel ingots and are applied to investigate the mechanisms for the formation of panel cracks. Panel cracking is an intermittent but persistent defect that causes affected steel ingots to be scrapped. A two-dimensional, finite-element, heat-transfer model was formulated and employed to calculate the temperature distribution in both large and small steel ingots during the various processing stages from initial casting to the start of rolling, including solidification, cooling in the mold and in air, reheating in the soaking pit, and subsequent air cooling. The stress state in the ingot arising from the calculated temperature variations was then determined. This involved the development of a transient, elasto-visco-plastic, finite-element, thermal stress model, including the effects of phase transformation volume changes and kinetics, creep, and temperature-dependent, mechanical properties. The results of the mathematical model predictions of temperature and stress were then used to determine the mechanisms and to suggest solutions for two different types of panel crack formation. Mid-face panel cracks apparently form during air cooling when the mid-face surface temperature is between the Ar_1 and 500°C. Off-corner panel cracks appear to initiate internally during the early stages of reheating but do not propagate to the surface until much later.

Modeling and Control of Casting and Welding Processes TMS American Institute of Mining, Metallurgical and Petroleum Engineers Conference Proceedings, Santa Barbara, CA, Jan. 12-17, S. Kou, R. Mehrabian, Eds., 1986, pp. 479-495

Introduction

Panel crack formation in static-cast steel ingots is a defect that has been plaguing the steel industry for several decades. Although the problem is intermittent, it is also serious since affected ingots must be scrapped. Panel cracks are manifested as two distinct types of cracking problems. "Mid-face" panel cracks are found exclusively in small, 2 to 6 ton, medium carbon steel (0.3 to 0.7% C) ingots and usually exhibit a single, continuous, longitudinal crack down the center of one of the ingot faces as shown in Fig. 1 (1). "Off-corner" panel cracks often form roughly oval, discontinuous crack patterns on the wide faces of large, 20 to 30 ton ingots as seen in Fig. 2 (2). They affect only low carbon steels (0.1 to 0.2% C) with high manganese content. Both defects affect only aluminum-treated steels and are caused by a combination of intermediate temperature ductility loss involving aluminum-nitride precipitation and thermal stress generation. The ductility problem has received a good deal of attention which was the subject of a recent review (3). The present study was undertaken to investigate the thermal stress aspects of the problem through the development of mathematical models of heat transfer and stress generation in static-cast steel ingots. The ultimate objective was to elucidate the mechanisms of formation for both types of panel crack and to evaluate possible solutions to the problem.

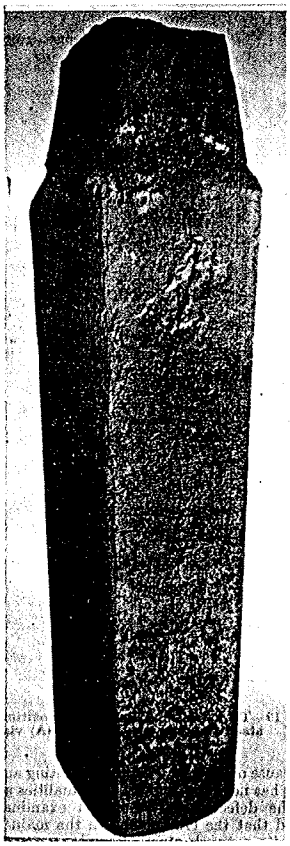

Figure 1 - Mid-face panel crack in 350 x 350 mm square En18 (0.4% C, 1.0% Cr) steel ingot (1).

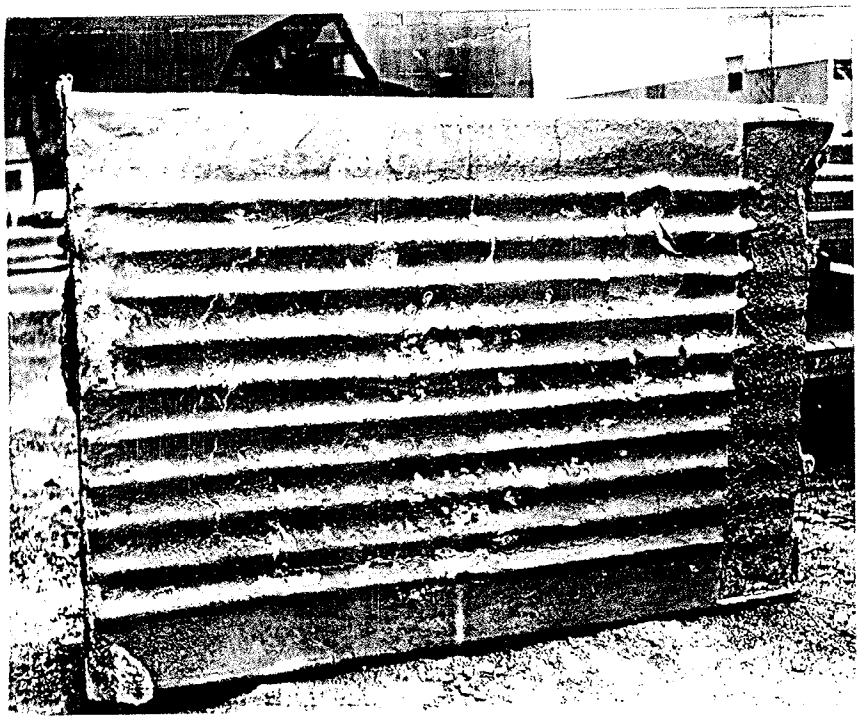

Figure 2 - Off-corner panel cracks in a 760 x 1520 mm, rectangular, corrugated (0.14% C, 1.4% Mn, Si-killed, Al grain refined) steel ingot (2).

Mathematical Heat-Flow Model

Since thermal stresses in the ingot arise solely from changing temperature gradients, the first step was to develop a mathematical heat-flow model. Because panel cracks are primarily longitudinal and exhibit two-fold symmetry, only one-quarter of a transverse, two-dimensional section through the ingot was considered.

Boundary Conditions

The 760 x 1520 mm ingot was chosen in Fig. 3 to present the boundary conditions for the heat transfer model. During the initial stages of solidification in the mold, heat is transferred from the solidifying steel shell to the interior surface of the mold by conduction using a heat transfer coefficient of 1700 W/m^2 K. This value was assumed to drop linearly to the time of gap formation whereupon heat is transferred via radiation alone. The time of gap formation, t_{gap}, was assumed to increase with increasing distance from the corner, d, according to a relationship based on empirical measurements by Oeters, et al. (4):

$$t_{gap}\ (s) = 50 + 10{,}800\ [d(m)]^{1.6}. \qquad (1)$$

Heat is lost from the exterior surface of the mold through radiation and natural convection to the ambient surroundings. Two-fold symmetry is imposed mathematically by setting the heat flow through the sides of the mesh representing ingot centerlines to zero.

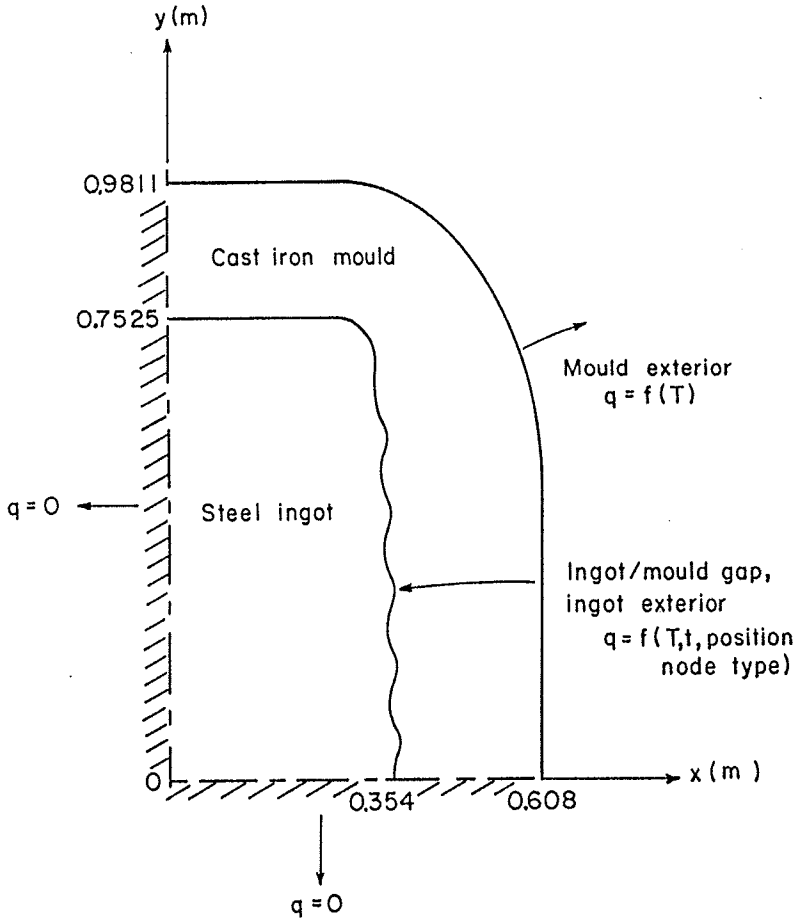

Figure 3 - One-quarter transverse section through a 760 x 1520 mm ingot and mold considered in the heat-flow model.

After stripping the ingot from the mold, heat is lost directly from the ingot surface by radiation and natural convection to the ambient surroundings. Finally, reheating of the ingot in the soaking pit is accomplished through radiant exchange with the soaking pit interior whose temperature was input as a function of time according to the desired reheating schedule.

Solution Technique

In order to include the effects of rounded corners and mold corrugations, a version of the finite-element method was employed. Three-node, linear-temperature, triangular elements were used and temperature-dependent thermo-physical properties were interpolated linearly within each element. Figures 4 and 5 show the finite-element meshes employed in the simulations for a small, square, mid-face panel-cracked ingot and a large, rectangular, off-corner panel-cracked ingot, respectively, together with their molds. The results of a previous comparison of numerical modeling techniques (5) indicated that this type of two-dimensional transient heat-conduction problem can be solved most effectively using the Matrix version of the finite-element method, coupled with the Dupont three-level, time-stepping scheme, specified heat-flux, (Neumann) lumped, boundary conditions formulated with property evaluation at the second time level, and the Lemmon technique for handling a latent heat evolution.

A computer program based on this method was coded in Fortran IV and run on the Amdahl 470 V/8, 12 megabyte computer at the University of British Columbia. Details of the computational procedure and temperature-dependent functions for the thermal conductivity and enthalpy of steel are given elsewhere (6).

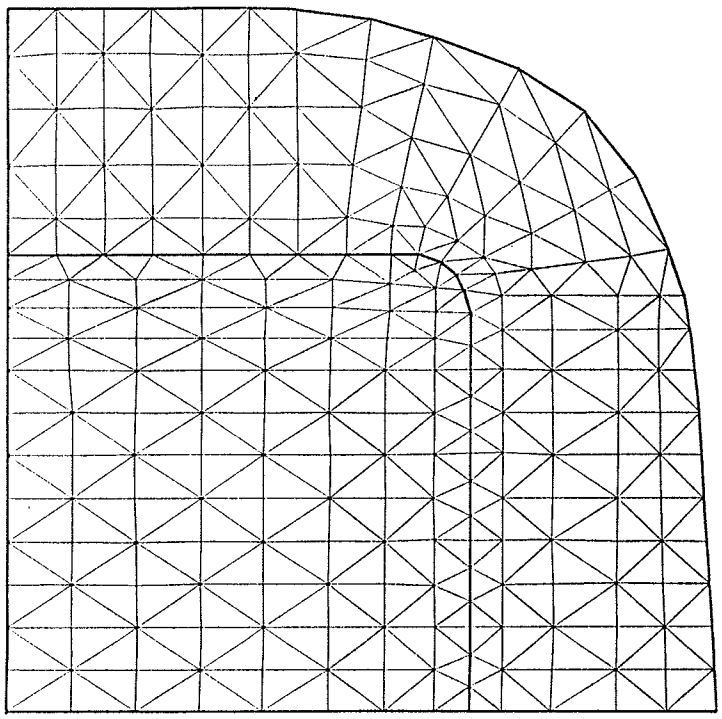

Figure 4 - Finite-element mesh for a 355 x 355 mm, two-ton, mid-face panel-cracked ingot and mold.

To distinguish the ingot surface from the mold surface at their common boundary, two different nodes with the same (x,y) coordinates were employed at each point along the interface. Each node that formed part of the ingot exterior surface exchanged heat directly with its corresponding node on the mold interior surface. To save computation time while retaining accuracy, variable time steps were adopted, increasing from a minimum of less than 1 s to 30 s each time the surface underwent rapid temperature changes.

Verification

To verify the internal consistency of the model, the results from initial runs were checked against analytical solutions for two test problems described elsewhere (5). The maximum difference found at any time for either problem was less than 1.5% for the chosen mesh and time-step sizes.

The model was then formulated to calculate temperatures during solidification of a small, 230 x 405 mm steel ingot cast at Stelco for experimental temperature measurement. The results were again in reasonable agreement (6).

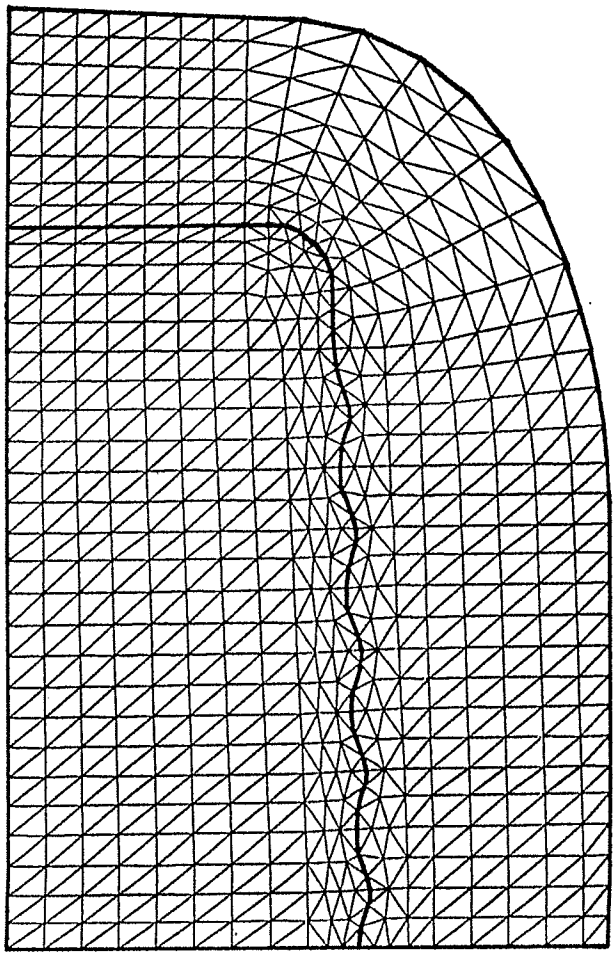

Figure 5 - Finite-element mesh for a 760 x 1520 mm, 25 ton, off-corner panel-cracked ingot and mold.

Mathematical Stress Model

An uncoupled, two-dimensional, transient, elasto-visco plastic, thermal stress model was then developed to determine the internal stress state of the ingot arising from the changing temperatures calculated by the heat-flow model. The same one-quarter transverse section of the ingot was considered and stresses in the mold were not computed. A state of plane stress was assumed and only small strains were considered.

Constitutive Equations

The total strain rate, $\dot{\varepsilon}$, was divided into three components:

$$\dot{\varepsilon} = \dot{\varepsilon}_e + \dot{\varepsilon}_T + \dot{\varepsilon}_p \qquad (2)$$

where $\dot{\varepsilon}_e$ and $\dot{\varepsilon}_T$ contain the elastic and thermal strain rate components, respectively. The creep and plastic strain rates were lumped together in $\dot{\varepsilon}_p$ since they are physically difficult to separate at elevated temperatures. The components of "plastic creep" strain rate, $\dot{\varepsilon}_p$, were calculated using the Prandtl-Reuses relations for associated plasticity as a function of the Huber-Von Mises total effective stress parameter, $\bar{\sigma}$, and temperature:

$$\dot{\varepsilon}_p = A_o \sinh(b\,\bar{\sigma})^n \exp(-Q/T). \qquad (3)$$

Coefficients for this equation were taken from tensile test data performed by Wray (8). For low carbon steel, the plastic creep strain rate in ferrite was enhanced by a factor of 1000 for temperatures below the Ar_3 in the ferrite/pearlite region. Within the two-phase region, a weighted average of the two plastic creep rates was employed based on the fractions of austenite and ferrite/pearlite present. Thus, the model must also track the phase fraction at every location.

Thermal strain was calculated incrementally as a function of the input temperatures:

$$\Delta\varepsilon_T = TLE(T_{t+\Delta t}) - TLE(T_t). \qquad (4)$$

The overall thermal linear expansion function, TLE, for a given steel was calculated using a weighted average of TLE for the fractions of austenite, γ, and ferrite/pearlite, α, structures present:

$$TLE = (\%\ \alpha)\ TLE_\alpha + (\%\ \gamma)\ TLE_\gamma \qquad (5)$$

The individual TLE_α functions were based on the temperature-dependent thermal linear expansion functions of the respective phases in pure iron modified to include the influence of carbon content on the expansion accompanying the $\gamma \rightarrow \alpha$ phase transformation (6). The kinetics of this phase transformation were also included through the use of separate functions for the austenite fraction present during heating and cooling. Since the continuous cooling transformation curves are relatively flat, for the slow cooling rates present in the ingot, these functions were characterized by the phase transformation start and finish temperatures on heating (Ac_1, Ac_3) and cooling (Ar_3, Ar_1) of the desired steel compositions, rather than by times. Figure 6 presents the critical portion of the overall thermal linear expansion function used for low carbon steel, and also illustrates the significant expansion that accompanies the $\gamma \rightarrow \alpha$ phase transformation. Details of this procedure are presented elsewhere, along with the exact temperature dependent functions for elastic modulus, thermal linear expansion and plastic creep strain rate that were employed (6).

Boundary Conditions

To impose two-fold symmetry, one degree of freedom was removed along each centerline, as shown in Fig. 7. The ingot center was fixed to prevent rigid body motion. A condition of zero stress was assumed over the remaining exterior surface of the ingot. This is reasonable since any stresses arising due to sticking in the mold, would occur early during solidification and lead to "hot tearing," a cracking problem involving high temperature embrittlement that is different from panel cracking.

Solution Technique

The stress model employs the finite-element method for spatial discretization, utilizing the mesh data from the heat-flow model as constant strain triangular elements. These simple elements were chosen over higher order elements because non-linearities, such as the discontinuous stress field over the solid-liquid boundary, would be better approximated by a large number of elements, than by fewer elements, each having more degrees of freedom.

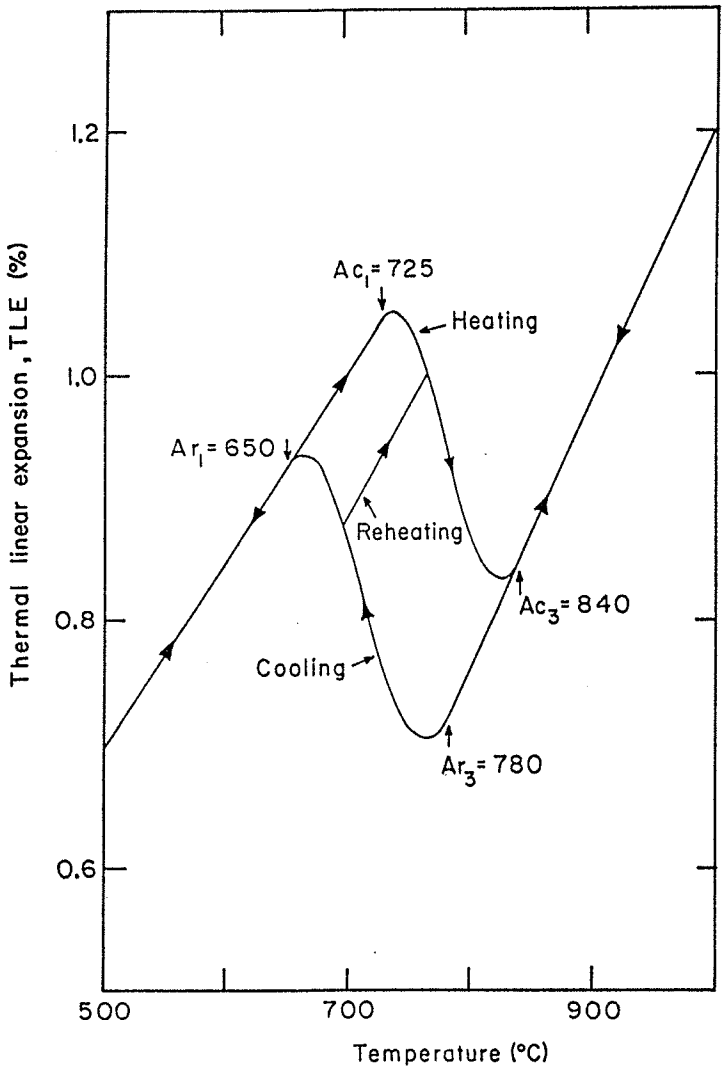

Figure 6 - Thermal linear expansion curves for the cooling and heating of low carbon steel assumed in the stress model.

An incremental procedure based on the visco-plastic model of Zienkiewicz and Cormeau (8) was employed to solve for the displacement and stress increments arising during each time step from the thermal and plastic creep strain load increments. Thermal strain increments for the time interval were evaluated using Eq. (4) and plastic creep strain increments from:

$$\Delta\varepsilon_p = \Delta t \, \dot{\varepsilon}_p \, (T, \bar{\sigma}_t) \tag{6}$$

An in-core routine using the Choleski method was employed to solve the resulting banded symmetric matrix equations. Finally, the stress, plastic strain and total strain increments calculated within each time step, as a function of the stresses and strains as the beginning of that time step, were accumulated; for example, by:

$$\varepsilon_{p_{t+\Delta t}} = \varepsilon_{p_t} + \Delta\varepsilon_p \tag{7}$$

The model uses a simple, explicit time-stepping procedure. Because the thermal and plastic strain vectors do not contribute directly to the stresses, and non-linearity is introduced into the problem mainly through these terms, minimization of a residual, "out of balance" force vector, was not very productive in improving accuracy. For this reason, it was found that accuracy improvement by iteration within a time step was best achieved by simply applying the thermal load in smaller increments, distributed throughout the time interval. This is equivalent to using smaller time steps and it allows all of the non-linearities in the problem to more closely approach the linear approximation inherent to the calculation procedure. Use of the same global stiffness matrix for several time steps allowed a substantial reduction in computing costs. Variable time step sizes

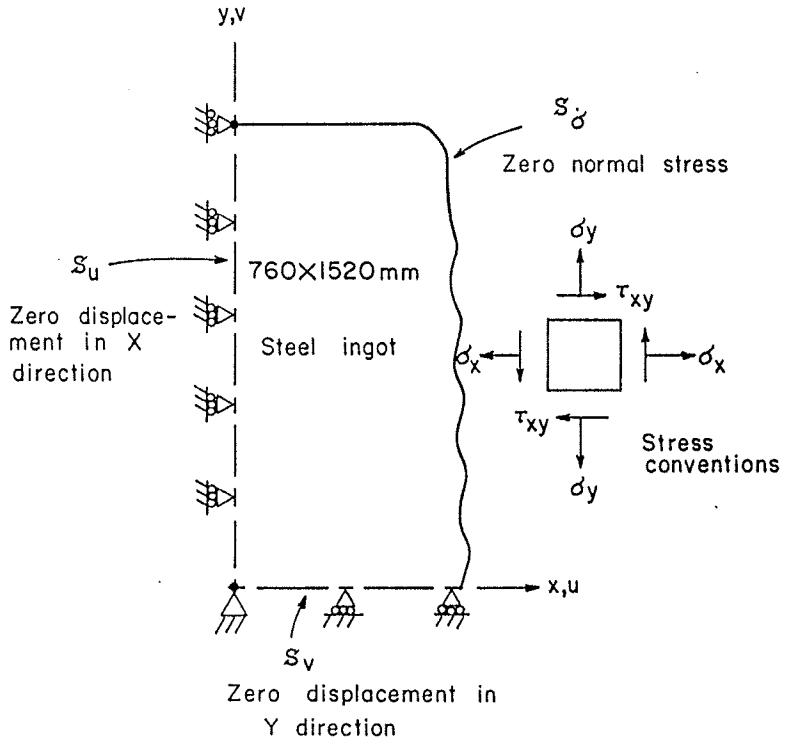

Figure 7 - One-quarter transverse section through a 760 x 1520 mm ingot and boundary conditions considered in the stress model.

were chosen in order to limit the maximum size of a plastic creep strain increment in any time step to five percent of the total effective plastic strain accumulated up to that time. The value of 5 percent falls within the 1-15 percent range suggested by Zienkiewicz and Cormeau (8) and was found to prevent instability in all cases.

Verification

The internal consistency of the model was verified through comparison of model predictions against analytical solutions for two test problems (6). One of these problems tested both the thermal strain and creep relaxation aspects of the stress model. An unconstrained beam subjected to a sudden parabolic temperature distribution was allowed to relax with time through a prescribed function for plastic creep. The asymptotical increase in plastic-strain gradually reduces stress in the beam to zero. The model stress predictions were consistently within 5 percent of the analytical solutions (6).

Results and Discussion

Fracture Criteria

Presentation of the results of a transient, two-dimensional, thermal stress model is made difficult by the vast amount of data generated. The task is linked to the problem of finding parameters that effectively quantify the stress state and adequately indicate the cracking potential.

The total strain is largely composed of thermal strain, which should not bear any direct influence on cracking tendency. Plastic creep strain, however, should be a logical fracture criterion. For a creep-void coalescence fracture mechanism, both tensile and compressive plastic strains contribute to structural damage so the increments of plastic creep strain already calculated using Eq. (6) were accumulated in a positive sense by

$$\bar{\varepsilon}_{p_{t+\Delta t}} = \bar{\varepsilon}_{p_t} + |\Delta\varepsilon_p| \qquad (8)$$

However, model simulations revealed that this effective plastic strain, $\bar{\varepsilon}_p$, rarely exceeded 2 percent at any location or time during the processing of either ingot. This reveals the importance of grain boundary embrittlement and strain concentration in the fracture mechanism.

For materials that yield, flow plastically, and subsequently fail in a ductile manner, the Von Mises effective stress parameter, $\bar{\sigma}$, based on maximum distortion energy, has been found to be a good fracture criterion:

$$\bar{\sigma} = (\sigma_x^2 + \sigma_y^2 + 3\tau_{xy}^2 - \sigma_x \sigma_y)^{1/2} \qquad (9)$$

However, regardless of their cause, cracks can only propagate and open up under tension. To distinguish regions of tension and compression, this parameter, $\bar{\sigma}$, was therefore assigned a negative value if the greatest principal stress was compressive. It is displayed graphically as iso-stress contour lines using a linear interpolation technique within elements. Temperature results are displayed in the same manner.

Finally, to visualize the simple fracture criterion of maximum normal stress, principal stresses were calculated:

$$\sigma_{I,II} = \frac{\sigma_x + \sigma_y}{2} \pm \left[\left(\frac{\sigma_x + \sigma_y}{2}\right)^2 + \tau_{xy}^2\right]^{1/2} \qquad (10)$$

Because the columnar grain boundaries, growing perpendicular from the ingot surface, are known to be weak, the orientation of the stresses is also important. The principal stresses were, therefore, presented graphically as stress bars plotted at each node in the mesh. The bars are oriented in the directions of the principal stresses with lengths that are proportional to their magnitudes and compressive stresses are distinguished with tick marks at the end of each stress bar. When one of the principal stresses is aligned directly across the grain boundaries, it is referred to as the "normal stress."

Mid-Face Panel Cracks

Due to the uncertainty involved both in calculating absolute stress levels and in determining accurate fracture criteria, the results of the numerical simulations are interpretted in a qualitative manner. These results indicate that the development of major regions of tensile and compressive stress within an ingot during processing is directly linked to the expansions and contractions that accompany the progress of the two phase $\gamma \rightarrow \alpha$ transformation zone through the ingot. Figure 8 presents the temperature and principal stress patterns within a 405 x 405 mm ingot at the two most critical stages of stress development. The conditions used in this simulation are summarized in Table I.

After one hour of air cooling (5400 s after casting), the center of the ingot faces or "mid-face," has partly transformed from austenite to ferrite. The two phase region is denoted on the temperature plot for this high carbon steel ingot by the Ar_3 and Ar_1 iso-temperature contours of 650 and 695°C, respectively. The expansion accompanying this transformation forces this region into a state of high compression. As the wave of compression passes completely beneath the exterior of the ingot, it is replaced by tension at the surface. The maximum tensile stress arises at the ingot surface 0.5 hours later (7200 s after casting), when the interior, expanding during transformation, is surrounded by a ferrite/pearlite exterior that is contracting as it cools. This time is the most likely for cracks to open up at the surface. The high tensile stress coincides with the temperature zone of embrittlement just below the Ar_3 (3). Networks of ductile ferrite, weakened by the presence of aluminum nitride precipitates, are surrounded by a strong pearlite matrix which produces strain concentration and intergranular failure of the ferrite along the prior austenite grain boundaries.

The importance of time in the development of the stresses is perhaps more clearly seen through examination of Fig. 9. This figure tracks the progression of both temperature and normal stress across the grain boundaries for the mid-face location where the panel cracks ultimately penetrate the surface.

Solidification and cooling in the mold produces compression at the ingot surface as the warm, interior seeks to contract while cooling within a rigid outer framework that is reheating. This surface compression persists during air cooling, after stripping at 0.5 hours, until 7000 s. From this time until 9500 s, this mid-face surface location experiences the highest stresses (over 50 MPa) and the highest plastic strains (almost 2 percent) of any location and time during processing of the ingot.

Of particular significance is the temperature range of this location between the Ar_3 and 500°C, over which the tensile stress persists. Below 500°C, accelerated contraction of the ingot interior, with respect to the already cool exterior, forces the surface back into compression, while

cracks are propagated deeper into the ingot. The final residual stress pattern at ambient temperature remains compression at the surface and tension in the interior, which has been verified by previous experimental measurements (9).

Figure 9 also shows the influence of carbon content, as indicated by the phase change temperature interval, on stress development. While the peak compressive stress closely follows the two-phase region, both the temperature interval and maximum extent of the tensile region remain relatively unaffected. Thus, the increased susceptibility of the higher carbon steels to mid-face panel cracks is related mainly to their lower ductility in this temperature range.

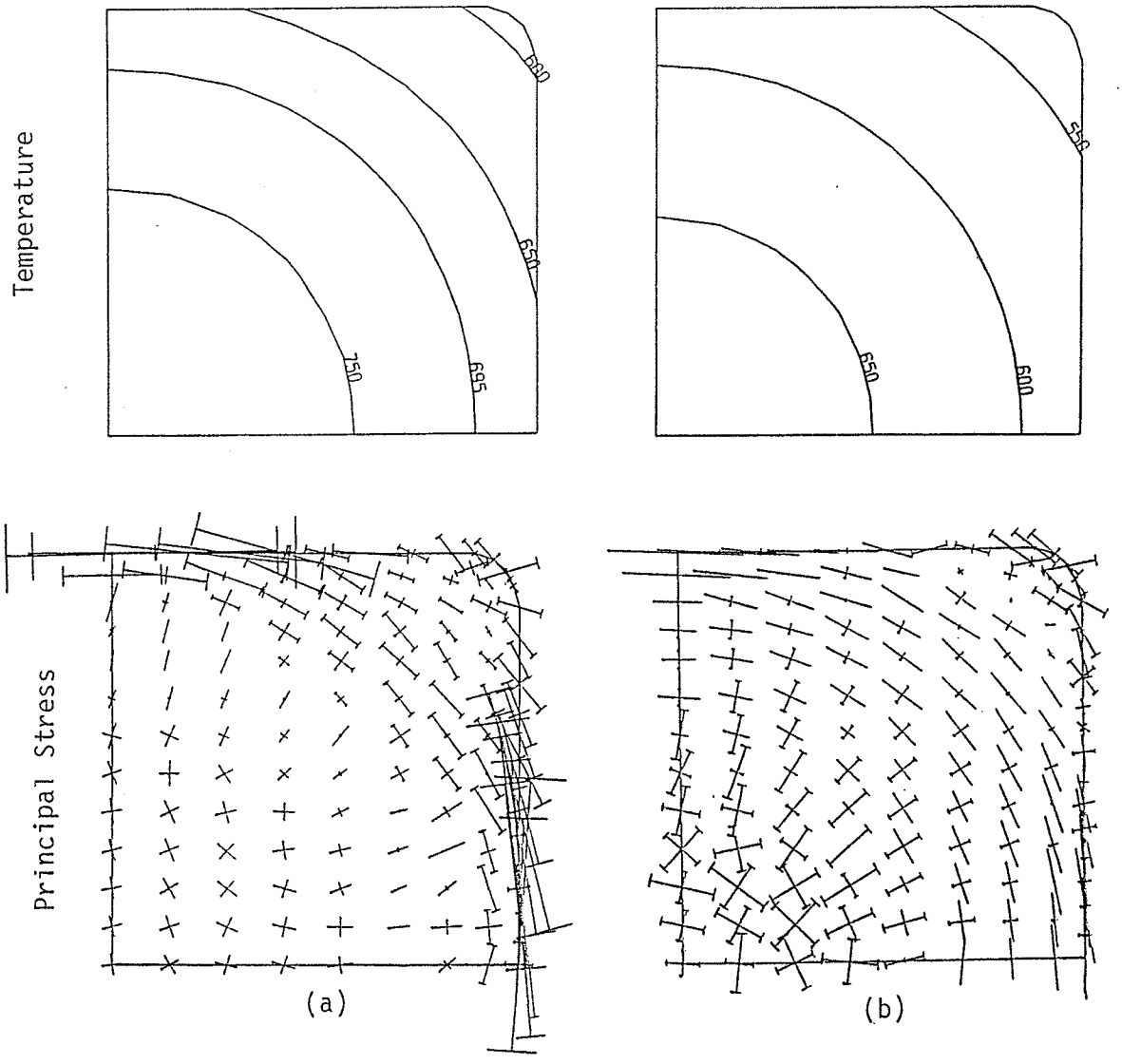

Figure 8 - Temperatures and principal stresses calculated by mathematical models for processing of a 405 x 405 mm ingot affected by mid-face panel cracks: a) 5400 s (1.5 hour) and b) 7200 s (2.0 hour).

Table I Processing Conditions Used for Model Simulations

Defect Simulated	Mid-Face Panel Cracks	Off-Corner Panel Cracks
Ingot Size	355 x 355 mm	760 x 1520 mm
Steel Composition	medium carbon steel 0.57% C, 0.65% Mn, 0.30% Si, 0.01% S, 0.01% P, 0.04% Al	low carbon steel 0.15% C, 1.50% Mn, 0.35% Si, 0.01% S, 0.01% P, 0.04% Al
Ar_1	650°C	650°C
Ac_1	720°C	725°C
Ar_3	695°C	780°C
Ac_3	760°C	840°C
Solidus Temperature	1410°C	1486°C
Liquidus Temperature	1480°C	1513°C
Initial Steel Temperature	1530°C	1530°C
Initial Mold Temperature	25°C	25°C
Strip Time	1800 s	14440 s (4 h)
Unjacketed or Air Cooling Time	---	6300 s (1.75 h)
Track Time	---	20700 s (5.75 h)
Initial Soaking Pit Temperature	---	1000°C
High Firing Time	---	12700 s (3.53 h)
Final Soaking Pit Temperature	---	1200°C
Total Time in Pit	---	49300 s (13.69 h)
Draw Time	---	70000 s (19.44 h)
Initial Time Step Size	0.9375 s	0.9375 s
Maximum Time Step Size	30 s	30 s

Off-Corner Panel Cracks

While mid-face panel cracks form during air cooling, off-corner panel cracks are more associated with reheating. Figure 10 illustrates the dramatic changes in both temperature and effective stress distribution that develop in a large, 760 x 1520 mm, ingot during the early stages of reheating. The conditions of this simulation were chosen to be conducive to panel cracking formation and are presented in Table I.

Prior to charging into the soaking pit, the development of stresses in the larger ingot are generally similar to that in the smaller ingot previously discussed. Figure 10 a) illustrates the position of the band of compression at the surface that accompanies the two phase zone, between the Ar_3 and Ar_1 temperatures of 780 and 650°C for low carbon steel, at the time of charging (20700 s), after 4 hours of mold cooling and 1.75 hours of air cooling. Within 20 minutes after charging, Fig. 10 b) shows how the rapid heating of the surface causes the Ac_3 isotherm of 840°C to wrap completely around the narrow face of the ingot. This encloses a region of two-phase material that is heating and contracting within a thin zone of retransformed austenite, that is expanding. The result is a temporary, subsurface tensile region, whose location near the corner and shape corresponds closely to the eventual location of off-corner panel cracks. Subsurface cracks are likely

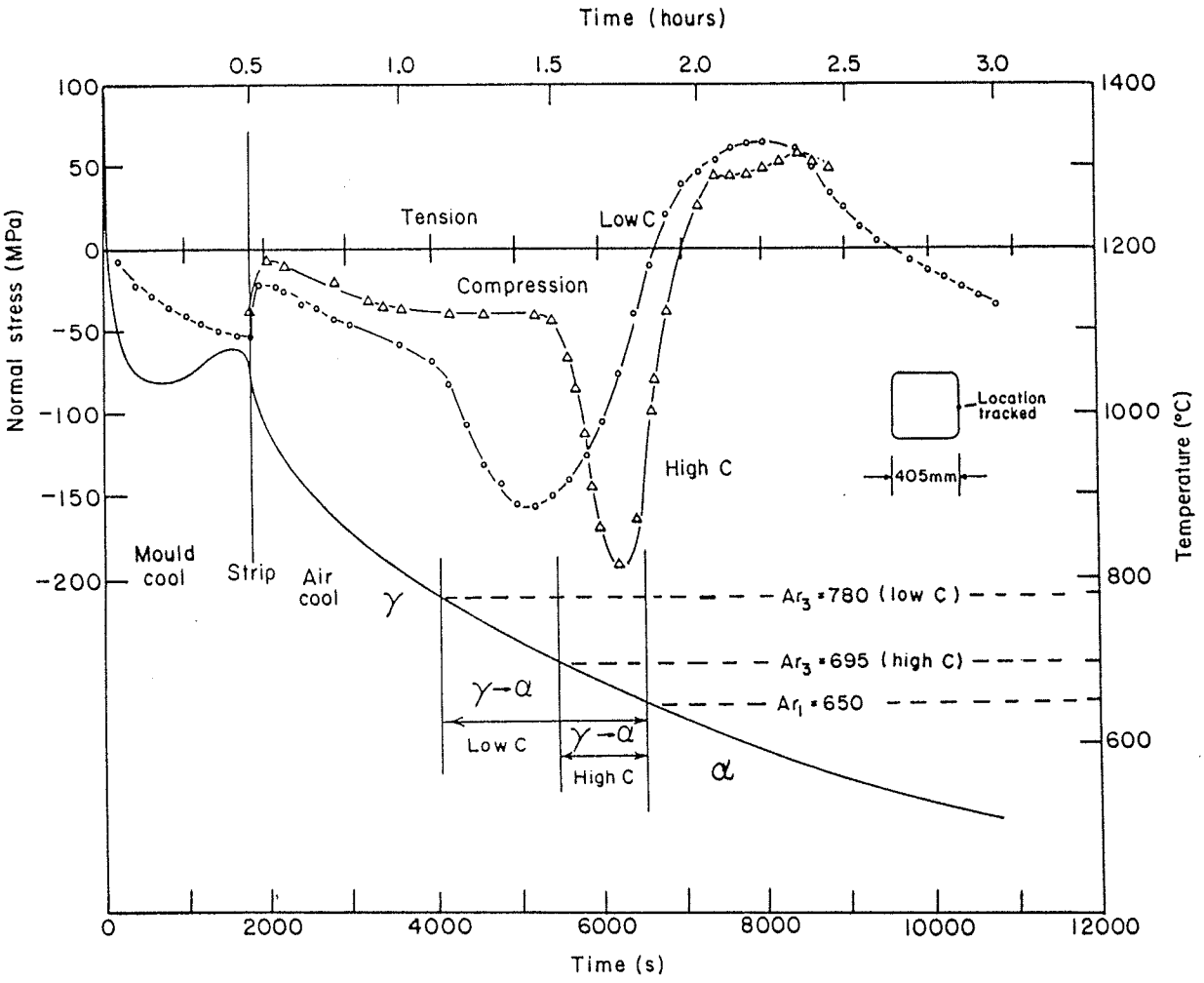

Figure 9 - Thermal and stress histories of mid-face surface (crack) location calculated by mathematical models for processing of 405 x 405 mm, mid-face panel cracked ingot.

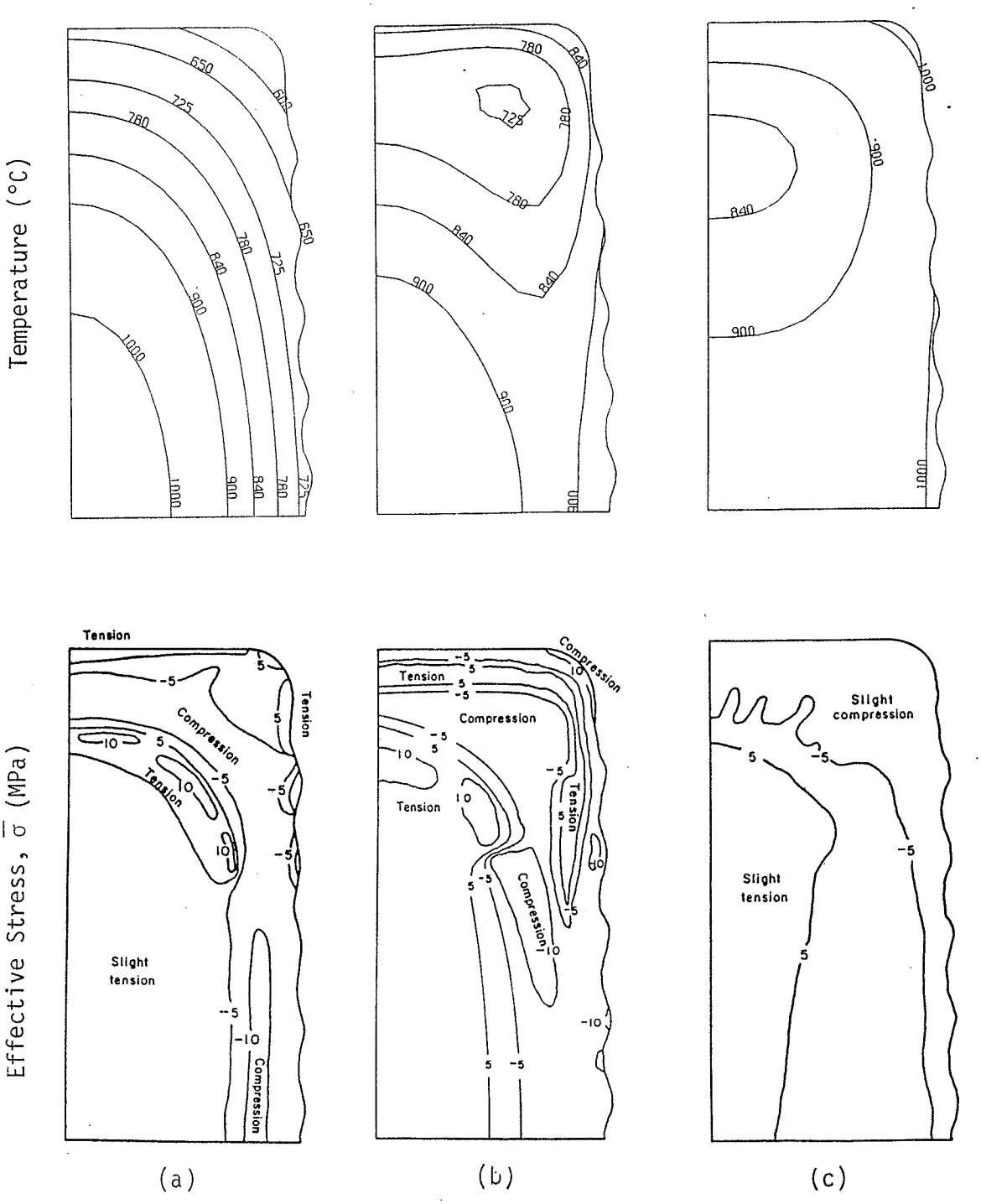

Figure 10 - Temperature and effective stress contours calculated by mathematical models for processing of 760 x 1520 mm ingot affected by off-corner panel cracks:
a) 20,700 s (charged after 4 hour mold cooling, 1.75 hour air cooling)
b) 21,900 s (20 minutes after charge)
c) 24,300 s (1 hour after charge).

to initiate here at this time because the temperature range just above the Ar_1 is susceptible to embrittlement by nitride precipitation at the austenite grain boundaries. A lack of extensive decarburization found on the crack surface suggests that the cracks do not propagate through to the surface at this time, however. This is because the thin zone of retransformed austenite is both under compression and has better ductility, after trapping the aluminum nitride precipitates harmlessly within new grains. Figure 10 c) shows that the subsurface tensile zone disappears a short time later, to be replaced by mild compression.

This sequence of alternating tension and compression can be seen more clearly in Fig. 11 at the critical location beneath the surface of the first corrugation trough from the corner. This figure presents the normal stress across the grain boundaries as a function of time during processing. It also presents the corresponding temperature history of this location so that the development of the phase transformations can be readily visualized.

The most significant feature of this graph is the presence of six distinct periods of tension during the entire processing history at this location. These six tensile peaks will now be examined in turn under the light of knowledge of metallurgical embrittlement to discover the mechanism behind off-corner panel crack formation.

Slight tension develops during solidification in the mold but the excellent ductility of steel above 1100°C can easily accommodate the resulting strains through creep. Immediately upon stripping, the contraction accompanying the rapid cooling of the ingot surface produces a second tensile peak. Adequate ductility is again expected to prevent deep crack formation at this time. This tensile zone then moves deeper into the ingot to be replaced by compression at the surface while the transformation to ferrite takes place at the austenite grain boundaries.

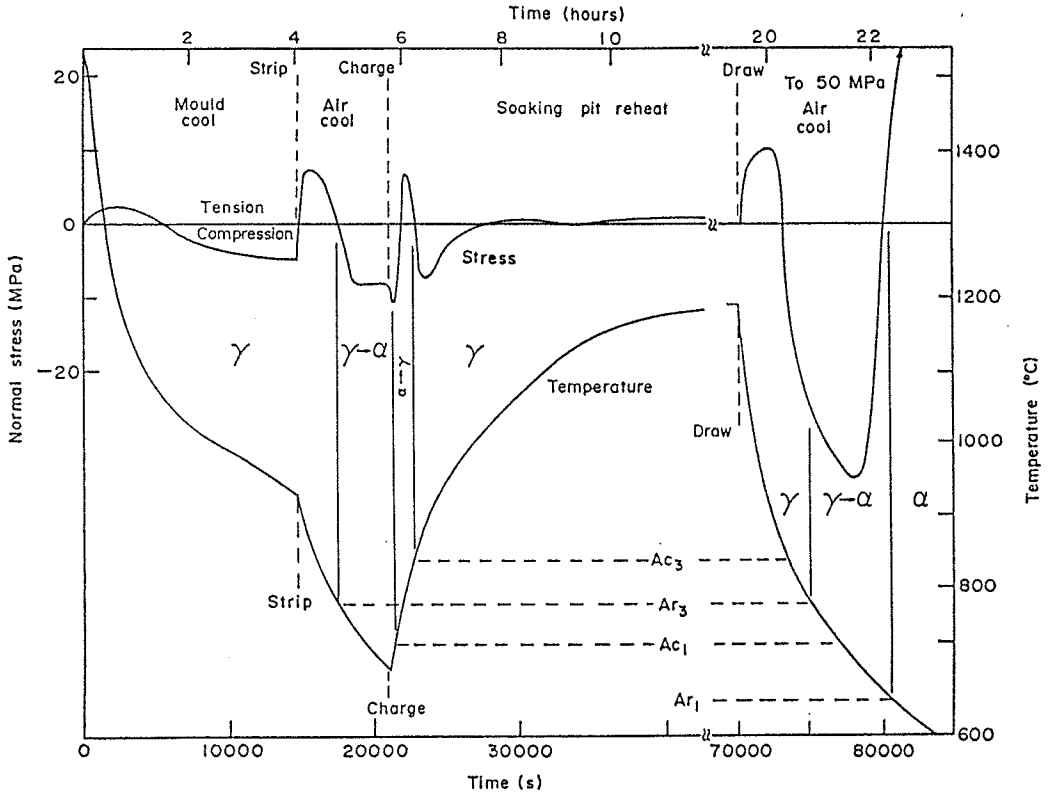

Figure 11 - Thermal and stress histories of off-corner subsurface locations calculated by mathematical models for processing of 760 x 1520 mm, off-corner panel cracked ingot.

When combined with sufficient time for aluminum nitride precipitation to embrittle the grain-boundary ferrite, the third tensile peak, arising during the early stages of reheating, is likely to initiate sub-surface cracks. This tensile peak corresponds to the subsurface tensile band illustrated in Fig. 10 b). The sensitivity of this tensile peak to processing conditions such as track time and reheating rate corresponds to the sensitivity of panel cracks themselves to thermal treatment. Short air cooling times, where the surface stays above the Ar_3, experience no third tensile peak. Long air cooling times and slow reheating rates cause the tensile peak to arise much later and deeper in the ingot. This offers further evidence that this third tensile peak is the critical factor in the formation of panel cracks. However, the cracks do not propagate through to the surface at this time, as explained earlier.

A fourth, very slight, tensile peak occurs for several hours during the latter stages of reheating. It arises as the cooler interior heats and expands within an equilibrated exterior. Plastic creep strains are the largest at this time, reaching 5 percent near the surface. However, this is unlikely to propagate the cracks without a severe loss in ductility. This could arise only under conditions of poor soaking pit operation that produce excessive temperatures and result in grain growth and strain concentration or local grain boundary melting.

Immediately after removal of the ingot from the soaking pit, a fifth tensile peak sweeps rapidly over the ingot surface as the austenite exterior contracts. Its characteristics are similar to the second tensile peak except the stress levels are higher. If the metallurgical integrity of the ingot had been reduced, then sub-surface cracks could propagate through to the surface along the weakened grain boundaries at this time.

Within 15 minutes after drawing the ingot from the pit, the surface has begun transformation and the corresponding expansion produces compression again. Usually, the ingot has been hot rolled by this time and the rolling stresses would further open up cracks. Deep, subsurface cracks that did not reach the surface could be welded shut and disappear. However, if the ingot was allowed to cool to ambient temperature instead, then it would experience a sixth tensile peak corresponding to the tensile zone, between the Ar_1 and 500°C, that produced mid-face panel cracks. The absolute stress levels in the larger ingot are higher at this time than at any other time during processing so would aggravate off-corner panel cracking in the worst cases.

Conclusions

Mathematical models for heat transfer and stress generation in static-cast steel ingots have been developed. These models were then applied to investigate the mechanisms of formation of two distinct types of panel cracks. Based on the results of the numerical simulations and previous work of the cracking problems and hot ductility of steel, solutions to both of these problems can be suggested.

Mid-face panel cracks appear to arise during air cooling when the mid-face surface temperature is between the Ar_1 and 500°C. Thus, suggestions to avoid their formation are:

1. Prevent the mid-face surface from dropping below the Ar_3 temperature of around 700°C by reheating the ingot prior to excessive cooling.

2. Reduce tensile stresses over the critical temperature range between 500°C and the Ar_1 temperature by slow or unsymmetrical cooling.

3. Prevent the formation of ferrite networks and embrittling nitride precipitates by using less susceptible steel compositions.

Off-corner panel initiate internally beneath the edge of the wide face of the ingot during the early stages of reheating. However, they do not appear to propagate to the surface until the latter stages of reheating or during air cooling immediately upon removal from the soaking pit. Suggestions to prevent their formation are as follows:

1. Prevent the stresses responsible for the sub-surface cracks from developing during the early stages of reheating either by employing a short air cooling time or by reheating slowly from an initially cold pit.

2. Force the sub-surface cracks to form deeper inside the ingot, so that they are unable to penetrate the surface, by employing a longer air cooling time.

3. Prevent the final air cooling stresses from propagating the sub-surface cracks through to the surface by improving the ductility of the steel. This could be achieved by employing carefully controlled soaking pit practices that avoid excessive times and temperatures or by casting less susceptible steel compositions.

References

1. B. L. Biggs, "Austenitic Grain-size Control of Medium-Carbon and Carburizing Steels," JISI, August 1959, pp. 361-377.
2. B. G. Thomas, J. K. Brimacombe, and I. V. Samarasekera, "The Formation of Panel Cracks in Steel Ingots: A State-of-the-Art Review, Part II-Mid-Face and Off-Corner Cracks," accepted for publication in Trans. I.S.S., 1985.
3. B. G. Thomas, J. K. Brimacombe, and I. V. Samarasekera, "The Formation of Panel Cracks in Steel Ingots: A State-of-the-Art Review, Part I-Hot Ductility of Steel," accepted for publication in Trans. I.S.S., 1985.
4. F. Oeters, K. Ruttiger, and H. J. Selenz, "Heat Transfer in Ingot Pouring," Casting and Solidification of Steel, 1977, pp. 125-167.
5. B. G. Thomas, I. V. Samarasekera, and J. K. Brimacombe, "Comparison for Numerical Modeling Techniques for Complex, Two-Dimensional, Transient Heat-Conduction Problems," Metallurgical Transactions B, (15B), No. 2, 1984, pp. 307-318.
6. B. G. Thomas, "Investigation of Panel Crack Formation in Steel Ingots using Mathematical and Physical Models," Ph.D. thesis, University of British Columbia, Vancouver, Canada, 1985.
7. P. J. Wray, "Mechanical, Physical, and Thermal Data for Modeling the Solidification Processing of Steels," Modeling of Casting and Welding Processes, AIME Conference Proceedings, 1980, pp. 245-257.
8. O. C. Zienkiewicz, and I. C. Cormeau, "Visco-Plasticity-Plasticity and Creep in Elastic Solids--A Unified Numerical Solution Approach," Int. J. Numer. Methods in Eng., (8), 1974, pp. 821-845.
9. A. Roth, et al. Aluminum, Vol. 24, 1942, p. 206.